Simultaneous Pair Electronic Transitions in Yb_2O_3

Harvey J. Schugar,*[1] Edward I. Solomon,*[2] William L. Cleveland,[1] and Lionel Goodman[1]

Contribution from The School of Chemistry, Rutgers University, The State University of New Jersey, New Brunswick, New Jersey 08903, and the Department of Chemistry, Princeton University, Princeton, New Jersey 08540. *Received December 4, 1974*

Abstract: The single-ion electronic spectra of Yb_2O_3 ($4f^{13}$) over the temperature range 2–300 K have been measured and interpreted. Three allowed purely electronic absorptions and associated vibronic structure have been identified for Yb(III) ions at electric dipole (C_2) sites, and in part for Yb(III) ions at magnetic dipole (C_{3i}) sites. A number of weak absorption bands in the 450–490 nm spectral region have been assigned unequivocally to the simultaneous pair excitation of neighboring Yb(III) ions and have been analyzed in detail. The vibrational band shapes of these pair absorptions reflect those of the contributing single ion transitions. Pair spectra of Yb(III) in YbOF have also been observed, while those possible for YbF_3, $Yb(OH)_3$, and $LaYbO_3$ were too weak to detect. These results are attributed to structural as well as bonding features, and help to elucidate the nature of the pair absorption process. Finally, the case for SPE absorptions by interacting Cu(II) ions is reconsidered.

The absorption of light by pairs of interacting metal ions was first observed in $PrCl_3$ at energies corresponding to sums of single ion Pr(III) electronic levels.[3] A theoretical model for this simultaneous pair excitation (SPE) process was developed,[4] and later applied in a semiquantitative manner to the $PrCl_3$ data.[5] Similar processes that are associated with the interactions responsible for magnetic phenomena have been observed over a wide spectral region. These include the enhancement of spin-forbidden single ion absorptions and the observation of SPE absorption or emission bands in both antiferromagnetic crystals and molecular dimers.[6-12] Also related are the simultaneous spin flips on adjacent ions (2-magnon scattering)[13] and summation vibrations of adjacent chromophores in the ir region.[14] Most of the above studies have dealt with systems containing interacting transition metal pairs.

In order to study the SPE absorption process in detail, we have chosen to exploit the advantages of Yb(III) systems. Yb(III) has relatively simple, but interesting, single ion spectra in the 10,000-cm^{-1} region. Highly condensed Yb(III) systems of known structure are readily available in high purity, contain a variety of bridging ligands and bridging geometries, and have a wide spectral window which includes the entire SPE spectral region. For Yb_2O_3, it has been possible to relate unequivocally the SPE bands to the single ion electronic levels of the interacting Yb(III) ions. Additional studies of YbF_3, $Y(OH)_3$, $LaYbO_3$, and YbOF have shed light on the interaction mechanism. Finally, we consider the case for attributing the characteristic additional absorption band exhibited by strongly coupled Cu(II) pair to a SPE process.

Experimental Section

Powdered samples of Yb_2O_3, $Yb(OH)_3$, YbOF, and YbF_3 stated to be 99.9% pure were obtained from commercial sources[15] and were used as received. The single ion spectra of Yb_2O_3 were obtained from both pressed disks (KBr, CsCl, and TlCl gave identical results) and a single crystal that was polished to a thickness of 90 μ. SPE spectra were obtained from a 4 mm thick single crystal of Yb_2O_3[16] and from pressed disks of neat Yb_2O_3. The multiple reflections undergone by a light beam in traversing a ~0.7 mm thick disk resulted in three times the band intensities obtained with the crystal; the spectra were otherwise identical. The disks were prepared with a standard 13-mm (ir) pellet press and were soaked in mineral oil to reduce light scattering.

Low and medium resolution spectra were measured with Cary 14, Cary 17, and Spex 3/4 meter Model 1702 spectrometers, using quartz dewars of standard design. The Spex instrument was calibrated with first-order neon lines for the SPE region and second-order neon lines for the single ion region. The high resolution spectra were measured at 2 K on a 3.4-m Jarrell-Ash spectrometer equipped with a 30,000 line per inch grating and calibrated with first and second order iron lines. A quartz–iodine source was used for the single ion region, while a quartz–bromine source was used for the SPE region in order to avoid I_2 absorptions. Single ion energies obtained from densitometer tracings were processed with a third-order least-squares fitting routine based upon the iron line positions. Oscillator strengths were obtained from measurements on single crystals.

Emission was observed at 77 and 4.2 K from Y_2O_3 doped with Yb(III) (1:900). Y_2O_3 also forms the C-type oxide. The sample was prepared from $YbCl_3 \cdot 6H_2O$ and $YCl_3 \cdot 6H_2O$ stated to be 99.99% pure (Lindsay).[15] The addition of NH_3 to a solution of the chlorides in triply distilled water precipitated the mixed hydroxide. The hydroxide was collected by centrifugation, washed well with water, and fired in an alumina crucible at orange heat for 6 hr. The ir spectra of the product was free of OH absorption bands and was identical with that of Y_2O_3. $LaYbO_3$ was prepared by firing the mixed hydroxide at yellow heat (~1400°) for 14 hr. The mixed hydroxide was obtained by the treatment of an equimolar aqueous solution of the metal chlorides with NH_3. The intensities and d spacings of the product's powder diffraction pattern corresponded to those calculated from the crystal parameters and structure factors reported for $LaYbO_3$.[17]

Due to the low intensity of the SPE absorptions, long effective path lengths were required. Under these conditions, normally undetectable levels of trace rare earth impurities could be observed. Although the SPE bands of both 99.9 and 99.99% pure Yb_2O_3 were identical with those of the single crystal, a further experiment was undertaken in order to definitely exclude the possibility of assigning an impurity absorption as a SPE band. It was observed that even thick (~2 mm) pressed pellets of $Yb(OH)_3$ exhibited no detectable absorption in the SPE region. A sample of Yb_2O_3 prepared by igniting this $Yb(OH)_3$ sample at orange heat in an alumina crucible exhibited the characteristic SPE spectra. These experiments verified that the bands we have assigned to SPE absorptions are not due to other rare earth impurities.

Structural Details. (A) Yb_2O_3. Yb_2O_3, a C-type oxide, crystallizes with the bixbyite structure.[18] The crystal parameters[19] are: cubic; $I_a3 - T_h^7$; $a = 10.434$ Å; $u = -0.0321$; $d_{calcd} = 9.22$, $d_{obsd} = 9.17$ g/cm^3. The unit cell contains 48 oxide ions and 32 Yb(III) ions, of which 24 are located at C_2 sites and 8 at C_{3i} sites. Except for the small positional parameter (u), the hexacoordinate Yb(III) ions are surrounded by an essentially cubic oxide environment out of which two oxides related by either a face diagonal (C_2) or a body diagonal (C_{3i}) have been removed.[18,19] Each Yb(III) has 12 nearest neighbor Yb(III) ions that are connected by 6 single oxide and 6 double oxide bridges. Those Yb(III) ions at C_{3i} sites have only C_2 site nearest neighbors, while those at C_2 sites have eight nearest neighbors at C_2 sites and four at C_{3i} sites. There are twice

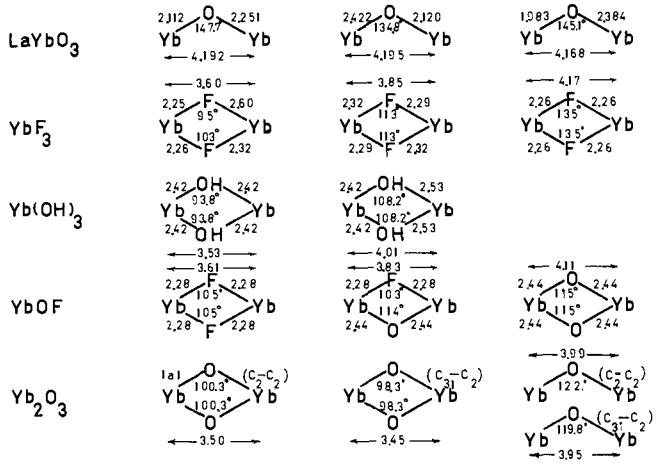

Figure 1. Geometrical features of the relevant Yb(III) pair-wise interactions in the compounds listed. All bond lengths and Yb-Yb separations are given in Å. Average Yb-O distance in Yb_2O_3 is 2.28 Å.

as many unique C_2–C_2 pairs as mixed C_{3i}–C_2 pairs. The geometrieof both types of pairs are shown in Figure 1.

(B) YbF_3. YbF_3 crystallizes with the YF_3 structure. The crystal parameters[20] are: orthorhombic; P_{nma}; a = 6.216, b = 6.786, c = 4.434 Å; d_{calcd} = 8.17 g/cm^3. Using the positional parameters for the similarly sized YF_3 lattice,[20] we have calculated that the nine-coordinate Yb(III) ions are surrounded by eight fluorides at ~2.3 Å and one at ~2.6 Å. Each Yb(III) ion has 12 "nearest" neighbor Yb(III) ions; the approximate Yb–Yb separations are: 3.60 Å (2×), 3.85 (2×), 4.17 (2×), 4.33 (4×), and 4.39 (2×). The geometries of some of these Yb pairs are shown in Figure 1.

(C) $Yb(OH)_3$. $Yb(OH)_3$ crystallizes with the UCl_3 structure. The crystals may be indexed as being hexagonal (C_{6h}^2 -$P6_3/m$) with a bimolecular unit cell described by $a = b$ = 6.22 Å, c = 3.50 Å, $\alpha = \beta = 90°$, $\gamma = 120°$, and d_{calcd} = 6.4 g/cm^3.[21] The Yb(III) ions are nine-coordinate, having six OH^- ligands at 2.42 Å and three at 2.54 Å. Each Yb(III) is connected by double hydroxide bridges to eight "nearest" neighbor Yb(III) ions; the Yb–Yb distances are: 3.53 (2×) and 4.01 Å (6×). The geometries of these Yb pairs are shown in Figure 1.

(D) $LaYbO_3$. $LaYbO_3$ crystallizes as a distorted perovskite. The crystal parameters[17] are: orthorhombic; C_{2v}^9-$Pna2_1$; a = 6.01, b = 5.81, c = 8.39 Å; d_{calcd} = 8.2 g/cm^3. Each Yb is coordinated to six oxide ligands (at distances of 1.98, 2.11, 2.12, 2.25, 2.38, and 2.42 Å) and has six nearest-neighbor Yb(III) ions linked by bent single oxide bridges. The geometries of the three similar types of Yb pairs are shown in Figure 1.

(E) YbOF. YbOF may be prepared as either a rhombohedral or a tetragonal phase.[22] The material used in our studies (Lindsay[15]) gave a powder diffraction pattern that indicated the presence of both phases. However, for the purpose of our studies, the structural differences between these phases are not critical.

The rhombohedral phase crystallizes in the space group $R3m$-D_{3d}^5 with a = 6.569 Å, α = 33.0°, and d_{calcd} = 9.25 g/cm^3.[22] We have used the positional parameters and crystal data of the isostructural and similarly sized YOF (a = 6.697 Å)[23] to calculate approximate bond distances in the YbOF lattice. The Yb(III) ions are coordinated to four oxides and four fluorides, the respective bond distances being 2.44 and 2.29 Å. Each Yb(III) is connected by double ligand bridges to 12 "nearest"-neighbor Yb(III) ions. Three are connected by double F^- bridges (Yb–Yb = 3.61 Å), six are connected by F^-/O^{2-} bridges (Yb–Yb = 3.83 Å), and three are connected by double O^{2-} bridges (Yb–Yb = 4.11 Å). Additional geometrical features of these pairs are shown in Figure 1.

Results and Discussion

Single Ion Spectra. (A) Background. The energy level diagram of Yb(III)(Xe4d^{10}4f^{13}5s^{2}5p^6) is relatively simple (Figure 2). Spin–orbit coupling splits the single ^2F term which arises from the 4f hole into $^2F_{7/2}$ and $^2F_{5/2}$ multiplets which are ordered in energy according to Hund's rule. These multiplets are separated in energy by $-7/2\ \xi$ where ξ is

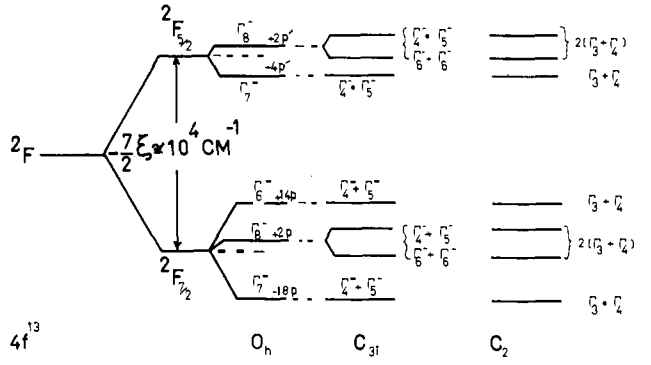

Figure 2. Correlation between the free ion levels of Yb(III) and those appropriate for the C_{3i} and C_2 lattice sites in Yb_2O_3. The relative splittings of the free ion multiplets by an O_h lattice site in terms of parameters p and p' have been obtained from ref 24. Γ's refer to Bethe's double group notation.

the spin–orbit coupling constant. Covalency effects present in Yb(III) compounds will cause a small reduction of ξ from the free ion value of 2883 cm^{-1}.

Electronic transitions between the $^2F_{7/2}$ and $^2F_{5/2}$ multiplets in the free ion are magnetic dipole allowed ($\Delta J = \pm 1$) and electric dipole forbidden. For the case of the C-type oxide, the crystal fields at the C_2 and C_{3i} sites will remove the $(2J + 1)/2$ Stark degeneracies of the free ion levels. Only the Kramer's degeneracy remains. Although the oxide sites are significantly distorted from cubic symmetry, it is useful to consider the cubic case as a starting point. The splitting of the free ion multiplets in O_h symmetry is shown in Figure 2. In the Bethe double group notation, Γ_6 and Γ_7 are doubly (Kramer's) degenerate, and Γ_8 is fourfold degenerate. The relative energies of the O_h terms are determined by the electrostatic interaction of the 4f hole with a cubic field and have been calculated in terms of the parameters p and P'.[24] These parameters do not include the effects of the $\langle r^6 \rangle$ splitting terms on the $^2F_{7/2}$ level.[25] While this omission could lead to a reversal of the $|^2F_{7/2}, \Gamma_8\rangle$ and $|^2F_{7/2}, \Gamma_6\rangle$ term ordering, their relative energies are not especially important here because we are primarily interested in only those transitions which originate from the lowest level of the ground electronic state.

A further reduction in symmetry from O_h to either C_{3i} or C_2 results in the splitting of the Γ_8 term; all terms now retain only a Kramer's degeneracy. Electronic transitions from the lowest $^2F_{7/2}$ level to the three levels of the $^2F_{5/2}$ multiplet are magnetic dipole allowed for the C_{3i} site and (forced) electric dipole allowed for the C_2 site. The total crystal field splitting within the $^2F_{5/2}$ and $^2F_{7/2}$ multiplets should be about 700 cm^{-1}. In principle, two sets of three transitions (i.e., one set for each site) are expected from the lowest $^2F_{7/2}$ level to the three Kramers' doublet excited $^2F_{5/2}$ levels. These transitions should be centered around 10,000 cm^{-1} and have a spread of ~700 cm^{-1}. Since the C_2 sites are statistically prevalent (3:1), and transitions originating at these sites are forced electric dipole allowed, they should dominate the observed spectra.

(B) Assignment of Single-Ion Spectra of Yb_2O_3. The single ion spectra of Yb_2O_3 in a pressed KBr pellet at 298 and 80 K are shown in Figure 3. In this section, we assign the three electronic transitions from these low resolution (~10 Å) spectra; the vibrational structure and true band shapes obtainable at higher resolution will be considered in the next section. All of the structure at lower energy than band C is seen to disappear at 80 K. It is clear that band C can unambiguously be assigned to the lowest energy doublet of the $^2F_{7/2} \rightarrow {}^2F_{5/2}$ transition. The A, B region is then assignable to hot bands originating from thermally populated

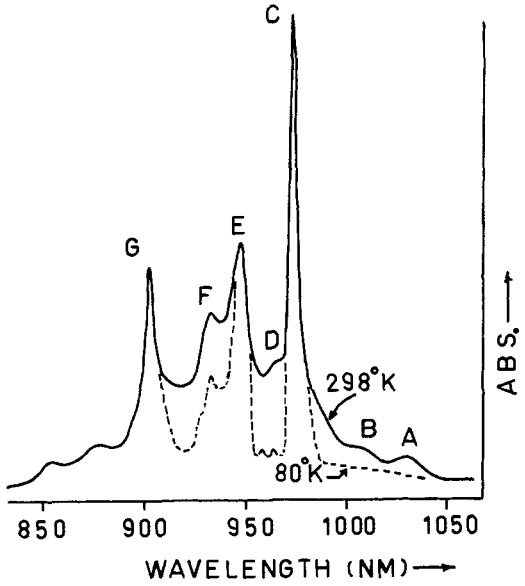

Figure 3. The single ion spectra at 298 and 80 K measured at low resolution (~10 Å) on a Cary 14. The Yb_2O_3 was dispersed in a pressed KBr disk.

Table I. Single Ion Transitions at 2 K Observed for Yb_2O_3 Oriented Along ⟨111⟩

Band	λ (Å)	(vac) cm^{-1}
C_1	9756.34	10,246.2 ± 0.4
C_1'	9746.03	10,257.8 ± 0.4
C_2	9655.06	10,354.4 ± 0.4
C_2'	9636.34	10,374.5 ± 0.4
C_3	9577.30	10,438.5 ± 0.4
C_3'	9567.11	10,449.6 ± 0.4
E_1	9505.10	10,517.8 ± 0.4
E_2	9484.14	10,541.0 ± 0.4
E_3	9466.10	10,561.1 ± 0.8
E_4	9422.97	10,609.5 ± 1.0
E_5	9404.76	10,630.0 ± 1.0
F_1	9366.23	10,673.7 ± 0.4
F_2	9344.44	10,698.6 ± 1.0
F_3	9326.75	10,718.9 ± 0.6
F_4	9298.65	10,751.3 ± 1.0
F_5	9229.12	10,832.3 ± 5.0
F_6	9205.47	10,860.1 ± 5.0
F_7	9159.69	10,914.4 ± 5.0
G_1	9026.38	11,075.6 ± 2.0
G_2	8746.4	11,430 ± 10
G_3	8562.4	11,676 ± 10

ground state electronic or vibronic levels. Cold bands may be expected at energies higher than C due to transitions from the ground electronic state to vibronic levels of the lowest energy doublet of the $^2F_{5/2}$ level. Since the metal-ligand force constants and lattice vibrations are essentially invariant to the well-shielded f-f transitions, hot and cold vibronic bands should be symmetrically arrayed about the first purely electronic transition. This feature of lanthanide spectra allows us to suggest that band A originates from an electronic level ~570 cm^{-1} above the ground state, since there is no cold band counterpart of A at C + 570 cm^{-1}. The most prominent band at a higher energy than C is band E (10,517.8 cm^{-1}). We can assign E to the transition from the ground electronic state to the second $^2F_{5/2}$ term. This assignment rests on the large intensity of E and the fact that it cannot be a vibration built on C. If E were vibronic, then a hot band corresponding to a substantially populated level at C − 250 cm^{-1} should be observable at 300 K. In addition, the low energy vibrations associated with E (see Figure 5 and Table I) are not present for band C. This is contrary to what would be expected if E were an intense fundamental built on C. There now remains the choice of either bands F or G for the third electronic origin. The problem of deciding which of four prominent absorption bands correspond to three allowable electronic origins has been well discussed for yttrium aluminum garnet doped with Yb(III).[24-27] The garnet spectra are quite similar to those of Yb_2O_3. The most recent interpretation of the garnet spectra corresponds to the choice of F as the third electronic origin and G as a vibration built upon C[26], based on the observation that F did not appear to have a hot band analog. Because of the numerous vibronic levels in this region, this argument may not be completely reliable. The assignment of the $^2F_{7/2}$ levels in the doped garnet using this technique is not in agreement with the results of electronic Raman studies.[28] In any event, the analogous assignment for the oxide (i.e., F being electronic and G being vibronic) would appear unlikely because the larger C-G energy spearation (~830 cm^{-1}) exceeds the energy of the observed lattice vibrations (Figure 6). It would then appear that G is either the third origin or a vibration built upon E or F. Alternatively, F is the third origin or a vibration built upon E or C.

The absence of a hot band at C − 428 cm^{-1} (~10% thermal population at room temperature) indicates that F is not likely to be a vibration associated with C. Similarly, the absence of a hot band at E −560 cm^{-1} rules against G being a vibration built upon E. The remaining choices are either G built upon F or F built upon E. It was hoped that these two possibilities could be distinguished by the temperature dependence of band D. Band D disappears at 80 K. Our best estimate of the Boltzmann energy of D is 180 ± 90 cm^{-1}, a value obtained from a linear log intensity ($\int I(\nu)\, d\nu$) vs. $1/T$ plot. This corresponds more closely to the E-F separation (~160 cm^{-1}) than the G-F separation (~400 cm^{-1}). Further confirmation of F arising from a vibration built upon E is indicated by the similarity in spacings of the low energy progressions centered on each band (24, 45, ~80 cm^{-1}). Thus F appears to be the fundamental in a ~156-cm^{-1} progression built upon E. The weaker absorption of a second 156 cm^{-1} quantum with similar substructure is also observable (next section). Band G, on the other hand, has no structure, which suggests that it corresponds to an excited state with an electronic wave function significantly different than those for E and F. In summary, our best estimate of the $^2F_{5/2}$ spacings are C-E = 272 cm^{-1} and E-G = 558 cm^{-1}. These experimentally obtained spacings correspond in Figure 2 to the significant distortion from O_h symmetry expected at the oxide sites, which leads to a large splitting of the Γ_8 quartet.

(C) Vibrational Structure. Having assigned C, E, and G as the three electronic origins, we shall attempt to explain the structure observed within these transitions. The band C region at higher resolution (~4 Å) is shown in Figure 4. As will be demonstrated in the next section, C_1 is the electronic origin of the Yb(III) ions at the C_2 sites while C_1' is that of those located at the C_{3i} sites. The C_1'-C_1 splitting of 12 cm^{-1} is found to be reproduced at 110 cm^{-1} (C_2'-C_2) and 190 cm^{-1} (C_3'-C_3) from C_1. Consequently, C_2 and C_3 (C_2' and C_3') can be assigned to 110 and 190 cm^{-1} vibrations built upon the first electronic transition of each site.

The E and F regions of the spectra are shown in Figure 5. Sets of vibrations that are similar in energy and shape are reproduced at ~156 cm^{-1} intervals which have an overall Franck-Condon factor $S \simeq 0.55$. This 156-cm^{-1} major mode is labeled as F_1 and F_5 which are built upon E_1. The subset of lower energy modes built on the 156-cm^{-1} vibronic origins are E_2, E_3, and E_4 built upon E_1; F_2, F_3, and F_4

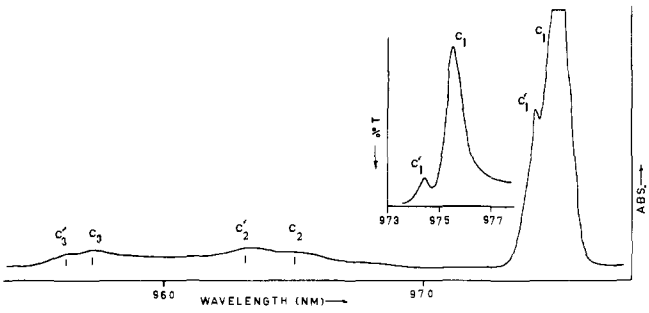

Figure 4. The band C region of the single ion spectra at 2 K of a 90 μ single crystal of Yb_2O_3 oriented along (111). These spectra were measured at ~4 Å resolution on a Cary 17 instrument. The insert shows the true C_1–C_1' separation obtainable at 4 K with the higher resolution (~0.1 Å) of the Spex 1702 single beam spectrometer. A Yb_2O_3–KBr pressed disk was used for this latter study. Energies of the C, E, and F band systems are listed in Table I.

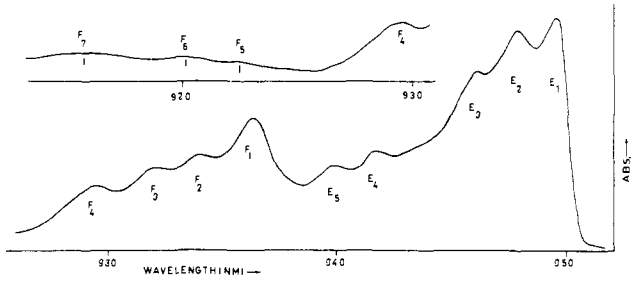

Figure 5. The E and F band systems of Yb_2O_3 (90 μ crystal) measured at 2 K. See Figure 4 caption for details.

built upon F_1; and F_6 and F_7 (much broader and weaker) built upon F_5. Thus, the first and second quantum of a ~24-cm^{-1} mode and one quantum of a ~85-cm^{-1} mode are observed. Only E_5 remains to be explained. It could be associated with either the first electronic origin C_1 (ΔE = 384 cm^{-1}) or the C_{3i} site. Finally, origin G_1 appears to have two vibrations built upon it: the first at 355 cm^{-1} and a second at 600 cm^{-1} (Figure 3).

Having experimentally obtained the vibrational frequencies associated with the electronic origins, it is now appropriate to consider the observed lattice modes. The T_h^7 Yb_2O_3 lattice has 5 × 16 × 3 = 240 vibrational modes of which only half are physically distinct. These modes transform as ($6\ A_{1g} + 6\ E_g + 30\ T_g + 8\ A_u + 8\ E_u + 36\ T_u$); the A_{1g}, E_g, and T_g modes are Raman active while the T_u modes are ir active. The observed Raman[29] and ir[30] spectra are listed in Figure 6. Since the macroscopic electric field due to the ionic character of the lattice transforms as T_u, the 36 T_u ir models are expected to be split at zone center into a doubly degenerate transverse (TO) and nondegenerate longitudinal (LO) branch. Light absorption will excite only the transverse modes. Consequently, the reflectivity spectra of Yb_2O_3 are needed to identify all of the ir active lattice modes. While such data are not available, they should closely resemble those reported for the isostructural Y_2O_3.[31] The reflectivity data of Y_2O_3, along with the ir and Raman data on Yb_2O_3, have been used to construct Figure 6. The large number of modes in the 80-620-cm^{-1} spectral region makes difficult the assignment of the electronically active vibronic modes. An additional complication arises because the fundamental ir and Raman modes are at $k = 0$ wave vector of the ∞ lattice. However, the electronically active vibrations can have any wave vector (k) contributing, weighted by the density of states which is larger near zone edge ($k = \pi/2a$ where a is the lattice constant). Since the lattice is fairly ionic, the energies at zone edge generally will be different from those at zone center. This expectation is supported by the observation of an overtone (not shown) of the 570-cm^{-1} ir band. Light absorption by two vibrations (1 and 2) requires only that $k_1 + k_2 = 0$ and will peak for the high combined density of states near zone edge. The observed overtone which peaks at 1080 cm^{-1} is 60 cm^{-1} lower than twice the zone center energy. Thus, even the higher energy modes which have been associated[29] with YbO_6 cluster vibrations show a significant energy dependence on k. Another argument against associating only the higher energy modes with "internal" vibrations of the cluster is that many of the observed electronically active vibrations are low in energy. Since the f–f transitions are localized, the vibrations of only nearest neighbor oxides should be electronically active. However, the observed vibrations span the low energy region down to 24 cm^{-1}. Therefore, the nature (and site symmetry) of the electronically active vibrations must be mixed. The presence of a 24-cm^{-1} vibronic progression implies one of the following: (a) the lowest energy observed vibration at ~80 cm^{-1} at $k = 0$ has a large negative dispersion to zone edge; (b) one of the ir or Raman inactive modes is in this region; or (c) the zone edge of some of the acoustic modes is at 24 cm^{-1}. The other observed electronically active vibrations all have possible assignments based on the observed vibrations of Yb_2O_3 listed in Figure 6.

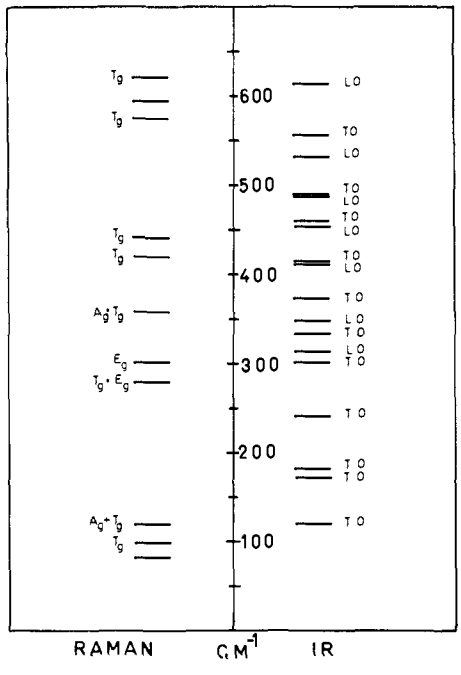

Figure 6. The observed Raman[29] and ir[30] vibrations of Yb_2O_3.

(D) Absorptions from Both Lattice Sites. We complete our assignment of the single ion spectra by experimentally demonstrating our previous assertion that C_1 and C_1' (Figure 4) corresponds to the first purely electronic $^2F_{7/2} \rightarrow {}^2F_{5/2}$ transition originating on the two different lattice sites. Since C_1' is readily observed at 80 K, it should not be associated with the magnetic ordering of the Yb_2O_3 lattice at 2.3 K.[19] Also, there is not a corresponding hot band for C_1' located at $C_1 - 11.6$ cm^{-1}. These observations are consistent with a two-site hypothesis. Evidence for C_1 and C_1' involving two different site absorptions comes from the temperature dependence of the emission spectra.

Probably because of concentration quenching, Yb_2O_3 itself does not emit down to 4 K. We have, however, doped (1:900) Yb(III) into Y_2O_3 which is isostructural as well as an excellent phosphor host. Rare earths doped in Y_2O_3 do not appear to show a site preference.[32] We observed that the doped oxide showed two sharp emission lines at 80 K at energies corresponding to C_1 and C_1'. When the tempera-

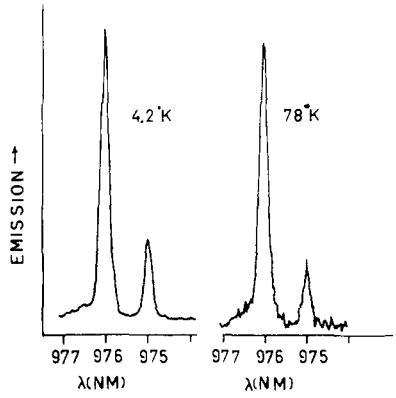

Figure 7. Emission spectra at 4.2 and 78 K of Yb(III) doped 1:900 into Y_2O_3. Spectra were measured at ~0.1 Å resolution on the Spex 1702 spectrometer. Emission corresponding to the C_1 and C_1' absorptions appears at 976.0 and 975.0 cm^{-1}, respectively.

ture was lowered to 4.2 K, both lines became more intense, although their relative intensities remained constant (Figure 7). If both lines corresponded to two levels of a given type of Yb(III), the line associated with the higher level should have markedly cooled out. The Boltzmann factor for an 11.6 cm^{-1} level at 4.2 K is $e^{-11.6/2.9} = 0.018$. The relative temperature independence of these resonant emission spectra establishes that C_1 and C_1' originate from Yb ions at different lattice sites. The oscillator strengths are $C_1 = 1.95 \times 10^{-7}$ and $C_1' = 0.15 \times 10^{-7}$, a 13 to 1 ratio. Since there are three times more C_2 sites than C_{3i} sites, and since the C_2 sites are forced electric dipole while the C_{3i} sites are only magnetic dipole allowed, we can associate C_1 with the C_2 site and C_1' with the C_{3i} site. Allowing for the 3:1 statistical factor, the ratio of the forced electric dipole to magnetic dipole intensity was found to be 4.3:1. A semitheoretical estimate of this ratio for Yb_2O_3 at room temperature yielded a value of 11:1.[33] Presumably, this qualitative agreement would have been better if the calculations were based upon spectral data obtained at low temperature in order to minimize odd parity vibrational effects.

The Pair Excitations. The absorption spectra of a ~1.6 mm thick pressed pellet of Yb_2O_3 powder in the spectral region 450–500 nm are presented in Figure 8. This region lies in the large spectral window between the Yb(III) single ion absorptions at ~10,000 cm^{-1} and the charge-transfer absorption edge at ~40,000 cm^{-1}. A number of weak bands (~10^{-3} as intense as the f–f absorptions) were observable even at room temperature. Cooling the sample to 80 K sharpened the spectra and caused a modest (~60%) increase in the band intensities. Measurements made at either 2.0 or 4.2 K under high resolution revealed no significant change in spectral features.

Because of the large effective light paths required to observe these weak bands, it was necessary to establish that they are not due to trace amounts of rare earth impurities (see experimental section). The noninvolvement of impurity absorption is further supported by an analysis of the energies and shapes of these absorption bands. The energies and assignments of the SPE bands (Figure 8) are listed in Table II. Assignments are based on the energy agreement with appropriate combinations of single ion excitations. Since the f–f excitations are well shielded from the Yb(III) environment by the filled 5s and 5p shells, SPE bands may be expected to correspond almost exactly with sums of single ion energies. Another consequence of the insulated f–f single ion excitations is that each partner of an excited pair can be considered to interact with its oxide nearest neighbors independently of the other. This allows us to factor out the single ion vibrational wave functions as was done in eq 4 (appendix). Thus, the shape of a pair transition is determined (eq 5, appendix) by the product of the Franck–Condon factors of the contributing single ion transitions. This effect is observed in the three curves extracted graphically from the complete SPE spectra. Curve I (Figure 8) contains all of the pair bands which have been assigned by reasons of energy additivity to combinations containing the lowest electronic origin C_1. Since C_1 is a sharp band, the SPE bands associated with combinations containing C_1 should have band shapes determined by the second single ion transition of the pair (i.e., $C_1 + C_1$, $C_1 + E_1$, $C_1 + G_1$). For this reason, curve I mirrors the shape of the single ion spectra (Figure 3). Curve II is built upon SPE bands involving the electronic origin E_1, which is associated with considerable vibrational structure. Thus, the SPE bands included in curve II are significantly broadened by the effect of E_1 on the product of the Franck–Condon factors, the band attributed to $E_1 + E_1$ being especially broad. The third indicated electronic origin G_1 is also fairly broad, which may be why we

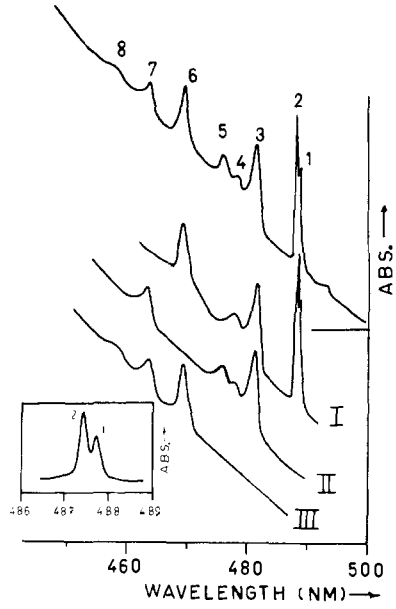

Figure 8. The SPE absorptions at 80 K of a neat Yb_2O_3 pressed pellet measured at ~1 Å resolution with a Cary 14 instrument. Band designations are given in Table II. Equivalent, although weaker, absorptions were exhibited by a 4 mm thick single crystal. Curves I, II, and III are those SPE absorptions built upon the C, E_1, and G_1 single ion electronic origins, respectively. The insert shows an expanded trace of the $C_1 + C_1$ and $C_1 + C_1'$ SPE bands.

Table II. Calculated and Observed Energies[a] of the SPE Absorptions in Yb_2O_3

SPE band	Observed energy[b]	Single ion combination	Calculated energy[c]
1	20,490.2 ± 0.4	$C_1 + C_1$	20,492.4 ± 0.8
2	20,503.6 ± 0.4	$C_1 + C_1'$	20,504.0 ± 0.8
		$[C_1' + C_1']$	20,515.6 ± 0.8
3	20,791 ± 3	$C_1 + E_1$	20,763.8 ± 0.8
4	20,932 ± 3	$C_1 + F_1$	20,919.9 ± 0.8
5	21,031 ± 5	$E_1 + E_1$	21,035.6 ± 0.8
6	21,327 ± 5	$C_1 + G_1$	21,321.8 ± 2.4
		$F_1 + F_1$	21,347.4 ± 0.8
7	21,592 ± 6	$E_1 + G_1$	21,593.4 ± 2.4
8	21,858 ± 7	$F_4 + G_1$(?)	21,826.9 ± 3
		$G_1 + G_1$	22,151 ± 4

[a] Energies in (vac) cm^{-1}. [b] Energies of 1 and 2 from single-crystal spectra measured at 2 K on 3.4 m Jarral Ash. Energies of 3–8 from spectra of neat Yb_2O_3 pellet at 80 K (see Figure 8 caption). [c] Based on data in Table I.

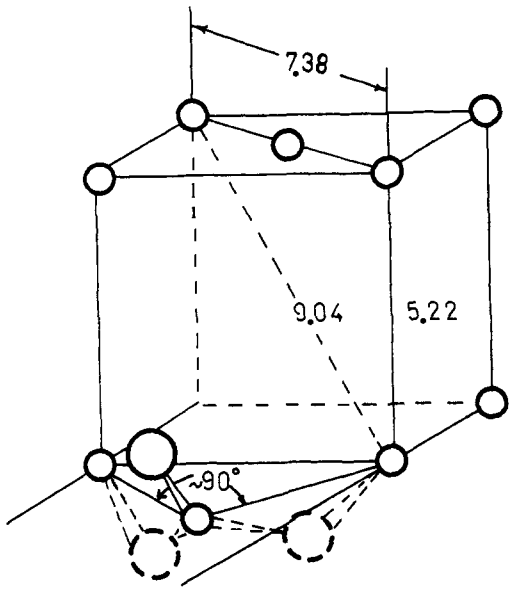

Figure 9. The eight C_{3i} sites in the Yb_2O_3 unit all lie at the corners of a 5.22 Å cube. Shown on the lower part of the figure is the mutually orthogonal oxide coupling of the nearest neighbor C_{3i} sites to a common C_2 site.

were not able to detect a SPE band corresponding to $G_1 + G_1$ above the background noise level.

A significant feature of the SPE spectra is the 13.4 cm^{-1} separation of bands 1 and 2. On the basis of energy additivity these SPE bands may be assigned to $C_1 + C_1$ and $C_1 + C_1'$. As described in the previous section, C_1 is the lowest electronic transition originating from Yb(III) at a C_2 site, while the C_1' transition is the analog for Yb(III) at the C_{3i} site. The absence of a $C_1' + C_1'$ SPE band is attributed to the C-type oxide structure of Yb_2O_3. Nearest neighbor pairs include both C_2–C_2 sites and C_2–C_{3i} sites. Yb(III) ions at different C_{3i} sites are not nearest neighbors, and can interact only via a common Yb(III) neighbor at a C_2 site. The exchange path for C_{3i}–C_{3i} pairs required by this arrangement is shown in Figure 9. This exchange path is unfavorable because of the intervening Yb(III) ion and the poor coupling afforded by the single oxide bridge relative to that of a double oxide bridge (see below).

The observed oscillator strengths of the first two SPE bands are $f_1 = 2.6 \times 10^{-10}$ and $f_2 = 3.54 \times 10^{-10}$. Since the numbers of unique C_2–C_2 and C_2–C_{3i} pairs are equal, the mixed C_2–C_{3i} SPE band has 1.35 times more intensity than its C_2–C_2 counterpart. The intensity of a SPE band is givenby the square of eq 3 (appendix). For an exchange induced interaction, this can be written approximately as $f_{SPE} = f_{CT}(J^2/\Delta E_{CT})$ where J is the exchange matrix element given by terms like those in eq 2 (appendix) and f_{CT} is the oscillator strength of the charge-transfer band which is at an energy E_{CT}. Thus, a small increase of $\sqrt{1.35} = 1.16$ in the interaction (J) between the C_2–C_{3i} pair over the C_2–C_2 counterpart would account for the observed intensity difference. We will not attempt a quantitative explanation of this difference. We do note that with the inclusion of the local oxide ligands, neither type of pair has any unique symmetry element. However, there are small physical differences between the pairs. For example, the Yb(III) ions in the mixed pairs are ~0.05 Å closer than those in the C_2–C_2 pairs. Using $f_{CT} = 1.0$ for the intense charge transfer (or perhaps f-d)[34] absorption edge of Yb_2O_3 at 40,000 cm^{-1}, we obtain $J(C_2\text{–}C_2) = 0.65$ cm^{-1} and $J(C_2\text{–}C_{3i}) = 0.75$ cm^{-1}.

Studies of Other Yb(III) Systems. In order to determine the effects of bridging ligands and geometries on the SPE absorption process, spectral studies were also done on pressed pellets of YbOF, YbF_3, $Yb(OH)_3$, and $LaYbO_3$. The structural details of these solids have been described (vide supra). Of these materials, detectable absorptions in the SPE region were observed only for YbOF. In comparison to Yb_2O_3, the SPE absorptions of YbOF were broader, with less structure, and qualitatively weaker. The broadness must in part be due to the presence of both rhombohedral and tetragonal YbOF (see Structural Details). The SPE spectra of YbOF corresponded in energy to summations of the prominent single ion excitations, and were not analyzed further.

The nonobservance of SPE absorptions in pressed disks of YbF_3, $Yb(OH)_3$, and $LaYbO_3$ is a significant finding. By increasing the thickness of the pressed disks to the limit set by light scattering losses, we estimate that the strength of the SPE absorptions of these latter compounds must be at least an order of magnitude weaker than those of Yb_2O_3. In order to observe such spectra above background noise, crystals of at least several centimeters thickness would be required.

As all of the compounds studied were ground into fine powders before being pressed into disks, the above results are not attributable to gross differences in particle size. Another factor that requires comment is the range over which the Yb pair concentration varies in the compounds studied. Ignoring for the moment the different types of Yb pairs, their concentrations are determined by the densities of the solids, the number of Yb ions per formula weight unit, and the number of nearest neighbor interactions that a given Yb experiences. The relative concentrations of Yb pairs are: Yb_2O_3(1.0), rhomb. YbOF (0.95), tetragonal YbOF (0.91), YbF_3 (0.76), $Yb(OH)_3$ (0.41), and $LaYbO_3$ (0.25). Therefore, the observed greater than tenfold decrease of SPE band intensities in the latter three materials cannot be attributed solely to a reduction in the number of pair interactions.

We consider next the specific geometrical features of these pairwise interactions. Both $LaYbO_3$ and Yb_2O_3 (half of the pairs) contain Yb ions linked in a similar manner by single bent oxide bridges (Figure 1). The average Yb–O lengths in both materials are similar. The Yb–Yb separations and Yb–O–Yb bridging angles are ~4.2 and ~4.0 Å, and ~140 and ~120°, respectively. With the removal of factors such as particle size and pair concentration effects, and the apparent unimportance of low temperature magnetic ordering (next section), we conclude that SPE absorptions in $LaYbO_3$ are intrinsically weaker than those in Yb_2O_3. Because of the similarity of the single oxide bridges in both materials, we further conclude that the Yb pairs linked by double oxide bridges in Yb_2O_3 must account for most of the observed SPE spectral intensity. The double oxide bridges differ from the single bridges in that the former are associated with more acute Yb–O–Yb bridging angles (~100°) and shorter Yb–Yb separations (~3.5 Å).

Common to the remaining systems studied is the feature of Yb ions linked by double ligand bridges, the Yb–ligand–Yb, bridging angles being 105 ± 10°. The only other material that exhibited SPE absorptions was YbOF, which contains three types of Yb ions linked by double ligand bridges. Based on the results obtained for Yb_2O_3 and $LaYbO_3$, those Yb ions linked by double oxide bridges in YbOF are a likely origin of the SPE absorptions. The broad SPE spectra (not shown) of YbOF appear to be somewhat weaker than those of Yb_2O_3. This result may be attributed to the fact that the number of neighbors joined by double oxide bridges per Yb in YbOF is four as compared to six in Yb_2O_3. Also, the corresponding Yb–O separations in YbOF (2.44 Å) are 0.16 Å greater than those in Yb_2O_3 (2.28 Å). The nonob-

servance of SPE absorptions in YbF_3 allows us to conclude that Yb ions linked by double F^- bridges are relatively less amenable to pair excitation. Each Yb in YbF_3 is linked by double F^- bridges to 12 neighbors; the resulting pair separations are : 3.60 Å (2×), 3.85 (2×), 4.17 (2×), 4.33 (4×), and 4.39 (2×). Based on our above conclusion that Yb ions separated by 4.11 Å and linked by double oxide bridges in YbOF give rise to observable SPE spectra, it follows that those in YbF_3 which are separated by 3.60, 3.85, and 4.17 Å are serious candidates for pair excitation. Even though each Yb has six sufficiently close neighbors, no SPE absorptions were observed.

Double hydroxide bridging is similarly ineffectual in promoting SPE absorptions. Each Yb in the $Yb(OH)_3$ structure interacts with neighbors that are located at distances of 3.53 (2×) and 4.01 Å (6×). The nonobservance of SPE absorptions in $Yb(OH)_3$ must be due to the nature of OH^-. In summary, the intensity of SPE absorptions in the above Yb compounds depends strongly on the nature of the ligand bridges and is relatively insensitive to the Yb–Yb distance. Double oxide bridges are clearly superior in this respect to double F^-, double OH^-, and single oxide bridges. Further implications of these findings are considered in the following sections.

Nature of SPE Absorption in Yb(III) Systems. The studies reported here bear on the nature of SPE absorptions in coupled lanthanide systems in two ways. First, the intensity of the SPE absorptions does not correlate with the known Yb–Yb separations in the compounds studied. This observation indicates that the mechanism of pair excitation does not depend on multipole type interactions or direct metal–metal overlap, both of which would lead to an increase in intensity with decreasing Yb–Yb distance. Second, the pronounced superiority of double oxide bridging over geometrically similar double F^- or double OH^- bridging indicates a superexchange type interaction. The contribution of a superexchange mechanism to the intensity of the SPE absorptions will depend on the extent to which the nearest neighbor Yb ions are coupled via the bridging ligands. The relative degree of Yb–ligand overlap should be related to the known covalency effects of the ligands. Such data are available from studies of lanthanide spectra in which the relative reduction of the free ion electron repulsion parameters by various ligands was found to be $S^{2-} > O^{2-} > I^- > Br^- > Cl^- > H_2O > F^-$.[34] Hydroxide should be similar to H_2O and F^- in this respect. Our spectral results with Yb_2O_3, YbOF, $Yb(OH)_3$, and YbF_3 can therefore be rationalized by the covalency effects of the ligands.

Thus an increase in covalency of the metal–ligand bond contributes to the pair intensity by increasing the exchange integral, J, between the two Yb(III) ions. Covalency also contributes to the intensity by lowering the energy of the ligand to metal charge transfer band, which reduces the energy denominator in the second-order exchange induced intensity mechanism

$$f_{SPE} = f_{CT}(J^2/\Delta E_{CT})$$

The above alone would indicate that $LaYbO_3$ should exhibit relatively intense SPE absorptions, although we were unable to observe any. Taking into account the types and densities of the pairs in Yb_2O_3 and $LaYbO_3$, the SPE transitions of the double oxide bridged pair are at least four times as intense as those of the single bridged pair. This must be due to an increase in the total effective Yb–Yb exchange integral, J, due to the presence of the two bridges. Each exchange interaction is proportional to a product of the metal overlaps with a given ligand orbital; the intensity of the SPE transition is then enhanced by the square of the total effective metal–metal exchange.

The effectiveness of the double oxide bridge in inducing pair transitions of Yb(III) is different from that found for transition metal pairs. In the former case the transitions are spin allowed, while the SPE absorptions studied in transition metals involved combinations of spin-forbidden transitions. Single, ~180° bridges were necessary in the latter case to induce strong antiferromagnetic coupling which overcame the spin-forbiddenness of the pair transition. Transition metal ion SPE intensities correlate with the degree of magnetic ordering; both decrease with increasing temperature. Although Yb_2O_3 undergoes magnetic ordering at 2.3 K,[19] the SPE spectra of Yb_2O_3 did not significantly change over the range 2–80 K and were easily observable at temperatures (300 K) where the extent of spin–spin correlation should be essentially zero.

In addition to the above considerations, there are also general differences between the SPE transitions of rare earth and transition metals due to the localized nature of the 4f as compared to the 3d wave functions. The J's must be smaller for the rare earths leading to much less SPE intensity. Also, the single ion energies are closely additive for SPE transitions of rare earth pairs, while there can be large interaction energies for SPE of transition metals.[36] The larger pair interactions of the transition metals can also eliminate the simple relationship between the shapes of the single ion and SPE absorptions we have observed for $Y6_2O_3$.

SPE Absorptions in Coupled Cu(II) Systems. In analogy to Yb(III) compounds, those of Cu(II) exhibit a relatively simple spin-allowed single ion spectra attributable to a single valence shell vacancy. Because the three d electrons are not shielded by higher filled valence shells, the Cu(II)–Cu(II) interactions in numerous dimeric, cluster, and lattice compounds are quite large relative to those in coupled Yb(III) systems. Furthermore, the oxidative character of Cu(II) results in fairly intense low energy (40,000 cm^{-1} or less) ligand → Cu(II) charge transfer excitations. Accordingly, the Dexter mechanism of SPE absorption[4] would indicate that such phenomena in coupled Cu(II) systems should be intense relative to those observed in the above Yb(III) systems. The presence of SPE absorptions in coupled Cu(II) systems has been suggested but not yet proven.

A variety of Cu(II) systems are known to exhibit antiferromagnetic or small ferromagnetic interactions. However, unlike the SPE processes involving the spin forbidden absorptions of other transition metal ions (Mn^{2+}, Cr^{3+}, etc.), antiferromagnetic ordering is not intrinsically required for SPE processes involving the ligand field bands of Cu(II). These magnetic interactions do, however, indicate the presence of metal–metal interactions necessary for the pair transitions.

In addition to the ligand field and charge transfer absorptions, a number of coupled Cu(II) systems exhibit, relative to reference monomeric magnetically dilute Cu(II) systems, additional absorption at somewhat less than twice the ligand field band energies. The most widely studied of such systems are the dimeric Cu(II) carboxylates, which have a characteristic absorption band at ~28,000 cm^{-1} not present in magnetically dilute Cu(II) carboxylates. The various assignments[37] of this absorption band include the suggestion of SPE absorption advanced by Hansen and Ballhausen,[38] which is supported by our results for Yb(III) systems. Relative to the Yb(III) systems, the large exchange and vibrational interactions between Cu(II) pairs should result in more intense SPE absorptions whose energies are less than those calculated from summations of single ion ligand field energies. A similar nonadditivity effect has been observed for the $^4T_{1g}(I) + {}^4T_{1g}(I)$ pair transitions of Mn(II) pairs in

$RbMnF_3$,[36] and should be larger for the dimeric Cu(II) carboxylates.

Other workers have observed absorptions at about twice the energy of the single ion transitions in other coupled Cu(II) systems. These include dimeric species such as

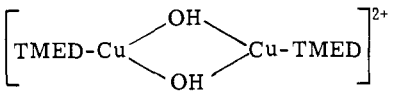

where TMED = $(CH_3)_2NCH_2CH_2N(CH_3)_2$,[39] and condensed Cu(II) fluorides such as $KCuF_3$.[40] In contrast to the dimeric Cu(II) carboxylates, the extra electronic absorption in these systems is less amenable to assignments which depend on the presence of either direct Cu(II)-Cu(II) overlap or symmetry restricted low energy charge transfer absorption. Of particular interest is an electronic spectral study of Cu(II) fluoride systems,[40] all of which exhibit ligand field absorptions centered at ~10,000 cm^{-1}. Systems such as CuF_2, $KCuF_3$, and heavily doped (>50%) Cu^{II}/ZnF_2 and Cu^{II}/MgF_2 show an addition absorption at ~20,000 cm^{-1}. Although this absorption band warrants further investigation, it is not easily attributable to an impurity absorption. Such an assignment is not supported by the doping experiments or by the observation that the 20,000-cm^{-1} absorption band of $NaCuF_3$, $KCuF_3$, and $RbCuF_3$ is either absent or weak in Na_2CuF_4, K_2CuF_4, and Rb_2CuF_4. Such behavior is consistent with the fact that the Cu(II) ions in a Na_2CuF_4 type lattice are essentially magnetically dilute whereas those in the $NaCuF_3$ type lattice show strong antiferromagnetic coupling.[41]

Acknowledgments. The single-crystal measurements at 2 K were made in the laboratory of Professor D. S. McClure (Princeton University). We thank him for his hospitality, helpful discussions, and interest in his study. We also thank Professor J. Potenza and Dr. J. A. Thich (Rutgers University) for assisting us in the calculations of the structural details of the compounds studied. We are grateful for the financial support of the Research Corporation (H.J.S.), National Science Foundation (E.I.S. and L.G.), and Lever Brothers (Fellowship to W.L.C.).

Appendix

Vibrational Band Shape of SPE Transitions. Described below is an extension of the Dexter model of the SPE process[4] to include vibronic Franck-Condon factors. Consider noninteracting ions A and B. The Born-Oppenheimer vibronic wave functions for the ground state, single ion excited states, and for the SPE state are given by equations 1a-c, respectively:

$$|\Psi_{ground}\rangle = |\Psi_A^0 \Psi_B^0 \chi_s^{00}\rangle \qquad E_{ground} = 0 \qquad (1a)$$

$$|\Psi_{single\ ion}\rangle = \left.\begin{matrix} |\Psi_A^e \Psi_B^0 \chi_t^{e0}\rangle \\ |\Psi_A^0 \Psi_B^e \chi_u^{0e}\rangle \end{matrix}\right\} \quad E_{single\ ion} = E_A^e, E_B^e \qquad (1b)$$

$$|\Psi_{SPE}\rangle = |\Psi_A^e \Psi_B^e \chi_v^{ee}\rangle \qquad E_{SPE} = E_A^e + E_B^e \qquad (1c)$$

$$|\Psi_{int}\rangle = \left.\begin{matrix} |\Psi_A^i \Psi_B^0 \chi_w^{i0}\rangle \\ |\Psi_A^0 \Psi_B^i \chi_x^{0i}\rangle \end{matrix}\right\} \quad E_{int}^{I} = E_i \qquad (1d)$$

and

$$\left.\begin{matrix} |\Psi_A^i \Psi_B^e \chi_y^{ie}\rangle \\ |\Psi_A^e \Psi_B^i \chi_z^{ei}\rangle \end{matrix}\right\} \quad E_{int}^{II} = E_i + E_{A,B}^e$$

The vibrational functions, χ_u^{0e}, χ_v^{ee} etc., have quantum numbers u, v, etc., appropriate to the potential surfaces constructed from the various Ψ_A Ψ_B states. In the Dexter treatment, the two-electron SPE transition is made electric dipole allowed (a one electron operator) by mixing the SPE and ground state at the first-order level, with an intermediate state $[\Psi_{inl}(d)]$ through electron-electron interactions, i.e.

$$|\Psi_{ground}\rangle^1 = |\Psi_{ground}\rangle + \sum_y \lambda_{00ie} |\Psi_A^i \Psi_B^e\rangle\langle\chi_y^{ie}|\chi_s^{00}\rangle|\chi_y^{ie}\rangle + \sum_z \lambda_{00ei} |\Psi_A^e \Psi_B^i\rangle\langle\chi_z^{ei}|\chi_s^{00}\rangle|\chi_z^{ei}\rangle \qquad (2a)$$

$$|\Psi_{SPE}\rangle^1 = |\Psi_{SPE}\rangle + \sum_w \lambda_{eei0} |\Psi_A^i \Psi_B^0\rangle\langle\chi_w^{i0}|\chi_v^{ee}\rangle|\chi_w^{i0}\rangle + \sum_x \lambda_{ee0i} |\Psi_A^0 \Psi_B^i\rangle\langle\chi_x^{0i}|\chi_v^{ee}\rangle|\chi_x^{0i}\rangle \qquad (2b)$$

where

$$\lambda_{00i0} = \frac{\langle\Psi_A^i\Psi_B^0|e^2/r_{12}|\Psi_A^0\Psi_B^0\rangle}{E_{int}^{II} + E^e} = [2\langle\Psi_A^i(1)\Psi_B^0(2)|e^2/r_{12}|\Psi_A^0(1)\Psi_B^0(2)\rangle - \langle\Psi_A^i(1)\Psi_B^0(2)|e^2/r_{12}|\Psi_A^0(2)\Psi_B^0(1)\rangle]/(E_{int}^{II} + E^e) \qquad (2c)$$

etc. In expression 2c the first term is the direct term which is employed by Dexter using a multipole expansion for $1/r_{12}$ and the second is the electron exchange term necessary for spin forbidden mixing.

The electric dipole transition moment for a SPE vibronic transition is given by

$$\bar{\mu}_{SPE} = {}^1\langle\Psi_{ground}|eR_i|\Psi_{SPE}\rangle^1 = \lambda_{eei0}\langle\Psi_A^0\Psi_B^0|eR_A|\Psi_A^i\Psi_B^0\rangle\sum_w\langle\chi_s^{00}|\chi_w^{i0}\rangle\langle\chi_w^{i0}|\chi_v^{ee}\rangle + \lambda_{ee0i}\langle\Psi_A^0\Psi_B^0|eR_B|\Psi_A^0\Psi_B^i\rangle\sum_x\langle\chi_s^{00}|\chi_x^{0i}\rangle\langle\chi_x^{0i}|\chi_v^{ee}\rangle + \lambda_{00ie}\langle\Psi_A^i\Psi_B^e|eR_A|\Psi_A^e\Psi_B^e\rangle\sum_y\langle\chi_s^{00}|\chi_y^{ie}\rangle\langle\chi_y^{ie}|\chi_v^{ee}\rangle + \lambda_{00ei}\langle\Psi_A^e\Psi_B^i|eR_B|\Psi_A^e\Psi_B^e\rangle\sum_z\langle\chi_s^{00}|\chi_z^{ei}\rangle\times\langle\chi_z^{ei}|\chi_v^{ee}\rangle \qquad (3)$$

Based on the real system under consideration (Yb_2O_3), further simplification of eq 3 is possible. Since the intermediate state is well separated from the SPE transition, we can assume closure over the intermediate vibrational states, i.e.

$$\sum_w|\chi_w^{i0}\rangle\langle\chi_w^{i0}| = \sum_y|\chi_y^{ie}\rangle\langle\chi_y^{ie}| = \ldots = 1$$

This would seem to be generally satisfied in that SPE transitions are found to be reasonably well separated to lower energies from the electric dipole allowed ($f = 1$) transitions. For Yb_2O_3 in particular, the SPE spectra at ~20,000 cm^{-1} are well removed from the absorption edge at ~40,000 cm^{-1}. Additional simplifications can be made when the interactions between the ions are small. The vibrational functions χ_v^{ee}, etc., can be regarded as harmonic oscillators having force constants appropriate to each of the noninteracting ions i.e.

$$\chi_s^{00} = \chi_{A_s}^0 \chi_{B_s}^0, \qquad \chi_v^{ee} = \chi_{A_v}^e \chi_{B_v}^e \qquad (4)$$

The approximation used in eq 4 requires that the single ion excitations do not cause large lattice distortions. This condition is best satisfied by the highly localized f-f transitions of the lanthanide ions. The approximation is less appropriate for systems such as MnF_2 in which the single ion transitions are more strongly coupled to the lattice. Because of Mn^{2+}-Mn^{2+} interactions via the F^- lattice, discrepancies of up to 400 cm^{-1} were observed between the energies of SPE bands and summations of contributing single ion excitations.[36]

The intensity of the SPE process is related to the square of the transition moment.

$$I_{SPE} \propto |\bar{\mu}_{SPE}|^2 = [\text{electronic part}]^2 \langle \chi_{A_s}{}^0 | \chi_{A_v}{}^e \rangle^2 \langle \chi_{B_s}{}^0 | \chi_{B_v}{}^e \rangle^2 \quad (5)$$

Equation 5 simply represents the SPE electronic intensity as given by Dexter[4] modified by a product of the Franck-Condon factors of the contributing single ion transitions.

References and Notes

(1) Rutgers University.
(2) Princeton University; address correspondence to this author at the Department of Chemistry, Massachusetts Institute of Technology, Cambridge, Mass. 02139.
(3) F. L. Varsanyi and G. H. Dieke, *Phys. Rev. Lett.*, **7**, 442 (1961); G. H. Dieke and E. Dorman, *ibid.*, **11**, 17 (1973).
(4) D. L. Dexter, *Phys. Rev.*, **126**, 1962 (1962).
(5) K. Shinagawa, *J. Phys. Soc. Jpn.*, **23**, 1057 (1967).
(6) C. J. Marzzacco and D. S. McClure, *Symp. Faraday Soc.*, **3**, 106 (1969).
(7) P. Day and L. Dubicki, *J. Chem. Soc., Faraday Trans. 2*, 363 (1973).
(8) H. J. Schugar, G. R. Rossman, C. G. Barraclough, and H. B. Gray, *J. Am. Chem. Soc.*, **94**, 2683 (1972).
(9) J. Glerup, *Acta Chem. Scand.*, **26**, 3775 (1972), and references therein.
(10) D. A. Dows and V. Schettino, *J. Chem. Phys.*, **58**, 5009 (1973), and references therein.
(11) E. Nakazawa and S. Shionoya, *Phys. Rev. Lett.*, **180**, 343 (1969).
(12) J. Ferguson, *Prog. Inorg. Chem.*, **12**, 241-244 (1970).
(13) S. R. Chinn, *Phys. Rev. B.*, **3**, 121 (1971); R. S. Meltzer, M. Low, and D. S. McClure, *Phys. Rev.*, **180**, 561 (1969).
(14) A. Burneau and J. Corset, *J. Chem. Phys.*, **56**, 662 (1972).
(15) Research Organic/Inorganic Chemical Corp., Sun Valley, Calif.; Lindsay Rare Earths, W. Chicago, Ill.
(16) This crystal was grown by the flame fusion technique at the National Lead Co., and was loaned to us by Professor McClure of Princeton University.
(17) von Müller-Buschbaum and C. Teske, *Z. Anorg. Allg. Chem.*, **369**, 255 (1969).
(18) L. Pauling and M. D. Shappel, *Z. Kristallogr., Kristallgeom., Kristallphys., Kristallchem.*, **75**, 128 (1930).
(19) R. M. Moon, W. C. Koehler, H. R. Child, and L. J. Raubenheimer, *Phys. Rev.*, **176**, 722 (1968).
(20) A. Zalkin and D. H. Templeton, *J. Am. Chem. Soc.*, **75**, 2453 (1953).
(21) R. W. G. Wyckoff, "Crystal Structures", Vol. 2, Interscience, New York, N.Y., 1967, p 78.
(22) K. Niihara and S. Yajima, *Bull. Chem. Soc. Jpn.*, **44**, 643 (1971).
(23) W. H. Zachariasen, *Acta Crystallogr.*, **4**, 231 (1951).
(24) R. Pappalardo and D. L. Wood, *J. Chem. Phys.*, **33**, 1734 (1960).
(25) M. T. Hutchings and W. P. Wolf, *J. Chem. Phys.*, **41**, 617 (1964).
(26) R. A. Buchanan, K. A. Wickersheim, J. J. Pearson, and G. F. Herrmann, *Phys. Rev.*, **159**, 245 (1967).
(27) D. L. Wood, *J. Chem. Phys.*, **39**, 1671 (1963).
(28) B. F. Argyle, R. L. Wadsack, and R. F. Chang, *J. Appl. Phys.*, **42**, 1478 (1971).
(29) G. Schaack and J. A. Koningstein, *J. Opt. Soc. Am.*, **60**, 1110 (1970).
(30) N. T. McDevitt and A. D. Davidson, *J. Opt. Soc. Am.*, **56**, 636 (1966).
(31) Y. Nigara, M. Ishigame, and T. Sakurai, *J. hys. Soc. Jpn.*, **30**, 453 (1971).
(32) J. Heber, K. H. Hellwege, U. Köbler, and H. Murmann, *Z. Phys.*, **237**, 189 (1970); H. Forest and G. Ban, *J. Electrochem. Soc.*, **116**, 474 (1969).
(33) W. F. Krupke, *Phys. Rev.*, **145**, 325 (1966).
(34) C. K. Jorgensen, R. Pappalardo, and E. Rittershaus, *Z. Naturforsch., Teil A*, **20**, 54 (1965).
(35) E. Dorman, *J. Chem. Phys.*, **44**, 2910 (1966).
(36) S. E. Stokowski, D. D. Sell, and H. J. Guggenheim, *Phys. Rev. B*, 4, 3141 (1971).
(37) L. Dubicki, *Aust. J. Chem.*, **25**, 1141 (1972).
(38) A. E. Hansen and C. J. Ballhausen, *Trans. Faraday Soc.*, **61**, 631 (1965).
(39) R. Näsänen, L. Lemmetti, and E. Vuori, *Suom. Kemistil. B*, **43**, 158 (1970). The absorption band at 360 nm observed by these workers for $[TMEDCuOH]_2(NO_3)_2$ is also exhibited by $[TMEDCuOH]_2(ClO_4)_2$. H. J. Schugar, unpublished observations.
(40) von O. Schmitz-Dumont and D. Grimm, *Z. Anorg. Allg. Chem.*, **355**, 280 (1967).
(41) von W. Rüdorff, G. Lincke, and D. Babel, *Z. Anorg. Allg. Chem.*, **320**, 150 (1963).

Radical-Anion Coordination of 9,10-Phenanthrenequinone in $Mo_2O_5(PQ)_2$

Cortlandt G. Pierpont* and Robert M. Buchanan

Contribution from the Department of Chemistry, West Virginia University, Morgantown, West Virginia 26506.

Received January 4, 1975

Abstract: The photochemical addition of 9,10-phenanthrenequinone (PQ) to $Mo(CO)_6$ in methylene chloride yields the diamagnetic complex $Mo_2O_5(PQ)_2$. Crystals of the complex are triclinic, space group $P\bar{1}$ with a = 13.024 (3) Å, b = 10.134 (3) Å, c = 10.389 (3) Å, α = 84.95 (4)°, β = 94.93 (4)°, and γ = 98.64 (4)°. Crystals form with one methylene chloride molecule per molecule of complex as solvent of crystallization. The structure was solved by conventional Patterson, Fourier, and least-squares procedures using X-ray data complete to 2θ = 50° (Mo Kα radiation). Refinement of the structure converged with final discrepancy indices of R = 0.045 and R_w = 0.054 for 3319 observed, independent reflections. Bonded to each Mo are two terminal oxo ligands with one oxygen bridging the two metals. Quinone ligands bond terminally to each metal through one oxygen with the second bridging the metals unsymmetrically. The complex molecule possesses approximate C_2 symmetry. Short Mo-O distances (1.68 Å) for the terminal cis oxo ligands are consistent with a complex of Mo(VI). Thus the quinones bond as magnetically coupled radical anions.

Complexes of 1,2-benzoquinones with transition metals have been known for many years but only recently have attempts been made to fully characterize their coordination properties. While 1,4-benzoquinones bond to metals as diene ligands,[1] 1,2-benzoquinones appear to bond exclusively through their oxygens. As such they may chelate to metals as oxidized benzoquinones (Ia), fully reduced catecholates (Ic), or as semiquinones (Ib). The 9,10-phenanthrene-

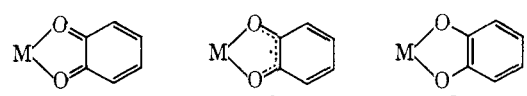

Ia Ib Ic